Measurement of Kaon Structure Function through Tagged Deep Inelastic Scattering (TDIS)

Kijun Park[1,†,*], Cynthia Keppel[1], Dave Gaskell[1], Alexandre Camsonne[1], Rachel Montgomery[2,†], John Annand[2], David Hamilton[2], Bjoern Seitz[2], Daria Sokhan[2], Kieran Hamilton[2], Tanja Horn[3,†], Dipangka Dutta[4], Garth Huber[5], Narbe Kalantarians[6], Charles Hyde[7], Sixue Qin[8], Craig D. Robert[8], Paul King[9]

[1] Jefferson Lab, Newport News, VA 23606, USA
[2] University of Glasgow, Glasgow G12 8QQ, United Kingdom
[3] Catholic University of America, Washington, DC 20064, USA
[4] Mississippi State University, MS 39762, USA
[5] University of Regina, Regina, SK S4S 0A2, Canada
[6] Virginia Union University, Richmond, VA 23220, USA
[7] Old Dominion University, Norfolk, VA 23529, USA
[8] Argonne National Laboratory, Argonne, IL 60439, USA
[9] Ohio University, Athens, OH 45701, USA

[*] Contact Person
[†] Spokesperson

Abstract

We propose to investigate the kaon structure function through Tagged Deep Inelastic Scattering (TDIS) by measuring small x_{Bj}, high Q^2 electrons scattered from a hydrogen target in coincidence with low momentum recoiling Λ hyperons reconstructed from decay protons and pions. The tagging technique allows for probing the strangeness content in the nucleon through its meson cloud, through the Sullivan process. This measurement will utilize the same experimental configuration as the $A-$ rated, $C1$ conditionally approved pion-TDIS (π-TDIS, PR12-15-006) experiment. The apparatus will consist of the Hall A Super BigBite Spectrometer (SBS) for electron detection, in conjunction with a low density target, and, a radial time projection chamber (RTPC) with

GEM-based readout, inside a large diameter 5T solenoid. These combined systems, along with the CEBAF high current CW beam, leverage the high luminosity and unique kinematics required to access the proposed physics. The low momentum tagging technique is crucial for the experimental separation of competing processes, leading to the isolation of the electron-meson scattering contribution. We will utilize the $D(e, e'p)n$ reaction to calibrate the RTPC for cross section measurements. This proposed experiment will be the first ever measurement to explore the elusive kaon structure function. Moreover, this process will be important to measure as it is a significant background to the pion TDIS measurement. The proposed measurement does not require additional beam time or detector to the approved running conditions of C12-15-006, and therefore can run as part of the pion-TDIS Run Group SBS.

Contents

1 Introduction

1.1 Physics Motivation

Simple quark models form a picture of the nucleon's structure in terms of its valence u- and d-quark constituents. The subsequent development of QCD clarified this picture, but should be modified to also include the contribution of the sea of virtual quark-antiquark ($q\bar{q}$) pairs and gluons (g), which made the nucleon a far richer and more dynamic environment. The structure of the nucleon structure in this context should not be limited to the light-quark $q\bar{q}$ sea, but also include local contributions of heavier quarks such as the strange or even charm quarks to the internal nucleon dynamics.

Chiral symmetry breaking in QCD is a fundamental feature of the nonperturbative dynamics of the quark and anti-quark sea, including strange and anti-strange quarks. While the generation of $s\bar{s}$ pairs through perturbative gluon radiation typically produces symmetric s and $\bar{s}$ distributions (at least up to two loop corrections [1]), any significant difference between the momentum dependence of the s and $\bar{s}$ parton distribution functions (PDFs) would be a clear signal of nonperturbative effects. In fact, insights from chiral symmetry breaking in the nonstrange sector led to the prediction [2] of an excess of $\bar{d}$ over $\bar{u}$ in the proton, which was spectacularly confirmed in DIS [3,4] and Drell-Yan [5, 6] experiments more than a decade later. A similar mechanism, which can be intuitively realized in the form of a pseudo-scalar meson cloud surrounding a valence-quark nucleon core, was subsequently used [7] to demonstrate the natural emergence of a nonzero $s\bar{s}$ asymmetry from the breaking of the chiral SU(3) symmetry of QCD. A recent study [8] provided a full detail of the calculation of the kaon loop contributions to the strange-quark PDF and its moments in the chiral effective theory. From the theory point of view, substantial studies have been discussed in terms of the formal derivation of the convolution representation, the various contributions from the lowest order diagrams, various regularization procedures that preserve the chiral and gauge symmetries of QCD, and form factors at hadronic vertices. From the effective chiral Lagrangian for parton distributions in the nucleon, twist-two quark operators with the hadronic operators are matched in the effective theory. The matrix elements of these operators are then related through the operator product expansion in QCD to moments of the PDFs. The results of the proposed measurement could contribute to the question if the valence distributions of the strange and non-strange quarks in the kaon is different and allow for comparing valence distributions in the kaon and pion.

Lattice QCD (LQCD) and Dyson-Schwinger Equation (DSE) calculations both predict that the valence up-quark distribution is significantly softer for the K^+ than for the π^+ [9]. On the other hand, the two calculations give different predictions of the total quark-momentum sum rule values for the two mesons. At a perturbative scale, the DSE quark-momentum sum rule prediction is 65% in the pion and 95% in the kaon. At the scale of the lattice spacing, LQCD predicts quark-momentum sum rule values of 52% for the pion and 66% for the kaon. Therefore, at a given scale, sea-quarks distributions carry their momentum approximately 5%, 0%, respectively. This indicates that the kaon has far less glue than the pion, which can be interpreted in various ways: 1/ heavier quarks radiate less readily than lighter quarks, 2/ heavier quarks radiate softer gluons than do lighter quarks, 3/ softer gluons have longer wavelength and multiple scattering are suppressed by interference, which is known as Landau-Pomeranchuk effect, 4/ Momentum conservation communicates these

effects to the kaon's u-quark. The recent full numerical calculations of DSE showed a good description of K/π ratio data from Drell-Yan experiment [10], which is shown in Fig. 1. In addition, the first DSE analysis estimated a small ($< 10\%$) contribution of gluon content in kaons.

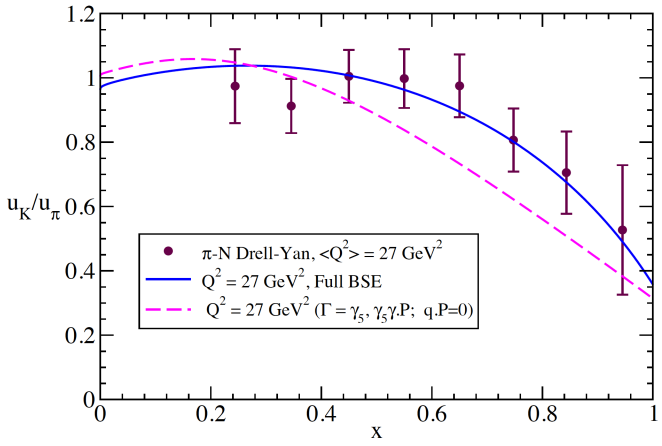

Figure 1: DSE prediction for the ratio of u-quark distributions in the kaon and pion [11]. The full Bethe-Salpeter amplitude produces the solid curve; the reduced BSE vertex produces the dashed curve. Data points from the Drell-Yan experiment [10].

In the limitation of calculation of PDFs at $x_{Bj} = 1$, asymptotic $x_{Bj} \to 1$ for spin-(in)dependent proton structure functions shows about 0.3, meanwhile both pions' and kaons' gluon and sea-quarks contents shows a dramatically increasing asymptotic Q^2 evolution, which can be only explained by pQCD splitting mechanism. The ratio $u_K(x)/u_\pi(x)$ is explained by immensely different gluon content in pions and kaons. Therefore, our proposed kaon-TDIS measurement together with the π-TDIS measurement is absolutely crucial to understand the distributions of quarks and gluons in the basic building blocks of nuclear matter.

In striking contrast to the sophisticated theoretical approaches, there is little experimental information at all on the parton distribution of the quark sea in the kaon. As explained in Section1.2 of the π-TDIS proposal [12], we will apply a ratio method to similarly extract the kaon structure function. For this study we will measure the semi-inclusive $H(e, e'\Lambda)X$ reaction, where Λ is the recoiled nucleon, denoted as the tagged structure function, F_2^T. The expected kinematic coverage will be in z and x_{Bj}, along with the measurement of the TDIS cross section. We will form the ratio R^T of the tagged (coincidence) to the DIS (singles) cross sections to measure the tagged structure function. Therefore, the kaon structure function F_2^K can then be determined from the measured tagged structure function F_2^T through $F_2^{(KY)}(x_{Bj}, z, k_\perp) = f_{KY}(z, k_\perp)F_{2K}(x_{Bj}/z)$ as was proposed for the pion structure function extraction. The present experiment will achieve 3% statistical and 5% systematic precision, roughly a factor of 3 improvement over [10].

1.2 Tagged Deep Inelastic Scattering (TDIS)

In specific kinematic regions, the observation of low-momentum recoil nucleons (hyperons) in the semi-inclusive reaction $eN \rightarrow e'YX$ can reveal features associated with correlated $q\bar{q}$ pairs (in particular $\bar{s}$) in the nucleon, referred to as the "nucleon's meson cloud", or the "five-quark component of the nucleon wave function". In particular, at low values of the four-momentum transfer squared $t \equiv k^2 = (N - Y)^2$ (shown in Fig. 2, where N and Y are the initial nucleon and final hyperon four-momenta, the cross section displays, according to current models, behavior characteristic of kaon pole dominance. Here, contributions from the exchange of non-pseudo-scalar quantum numbers ($J^P = 0^-$), such as vector mesons (ρ, ω) are suppressed, and the pole-effect of these heavier mesons is less pronounced in our kinematics, leading to a qualitatively different t-dependence than that arising from the kaon pole. Furthermore, the contribution from the three-quark component of the wave function is highly suppressed because the momentum of the recoiled hyperon peaks at $\approx$ 1 GeV/c. The JLab 12 GeV upgrade will provide the facilities for measurement of not only the mesonic structure but also the strangeness mesonic content in the nucleon. The electron Deep Inelastic Scattering (DIS) off the meson cloud of a nucleon target, the so-called Sullivan process [13], is illustrated in Fig. 2. This process is interpreted such that the nucleon parton distributions necessarily contain a mesonic parton content.

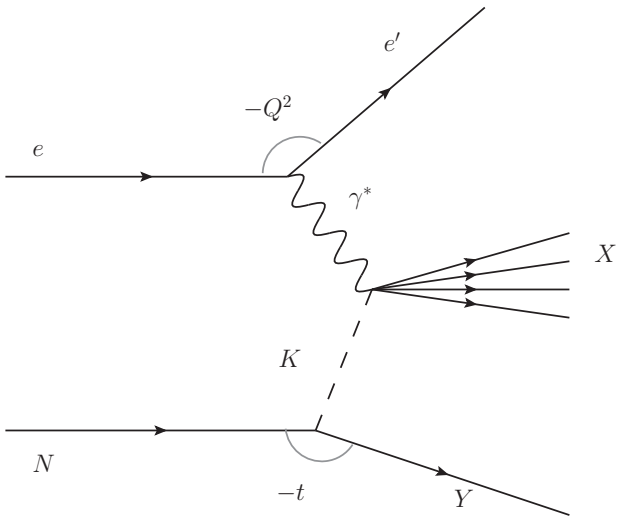

Figure 2: Feynman diagram for electron scattering from the kaon cloud of the hyperon Y, with the initial nucleon at rest (the Sullivan process).

To access the kaon partonic content via such a structure function measurement requires scattering from a meson target. The Sullivan process can provide reliable access to a meson target as t becomes space-like if the pole associated with the meson remains the dominant feature of the process. To check for pole-dominance, we will take data covering a range in t, and in particular at low t. A recent calculation [9] explored up to what values of t one may expect meson pole dominance. In the calculations, a virtuality eigenvalue for the bound-states was introduced into the Bethe-Salpeter equations to explore the off-shellness. For virtuality less than about 31, all changes in pion internal structure are linear and modest. A well-constrained extrapolation as used

in experimental analysis should be reliable. The next question is to address how the internal structure of the pion is modified. Figure 3 shows a detailed picture of possible rearrangements of the pion's internal structure from studying the impact of virtuality scalar functions. It presents the k^2-dependence of the ratio ($F_\pi^{virtual}/F_\pi^{real}$) of the leading Chebyshev moment for the ultraviolet (UV) dominant amplitudes. The results show that the impact of nonzero virtuality on the pion's internal structure is modest even at virtuality of about 31 (which corresponds to -$t \sim 0.6$ GeV^2) for length scales of greater/equal 0.2 fm. For length scales less than 0.1 fm, one observes plateaus describing nearly constant shifts in the amplitude. By repeating this analysis and expanding to kaon, $s + \bar{s}$ pseudo-scalar bound-state has been described. Interpolating to the pion, kaon masses, the off-shell correlation serves as a valid pion and kaon virtual targets correspond to $-t < 0.6$ GeV^2, $-t < 0.9$ GeV^2, respectively.

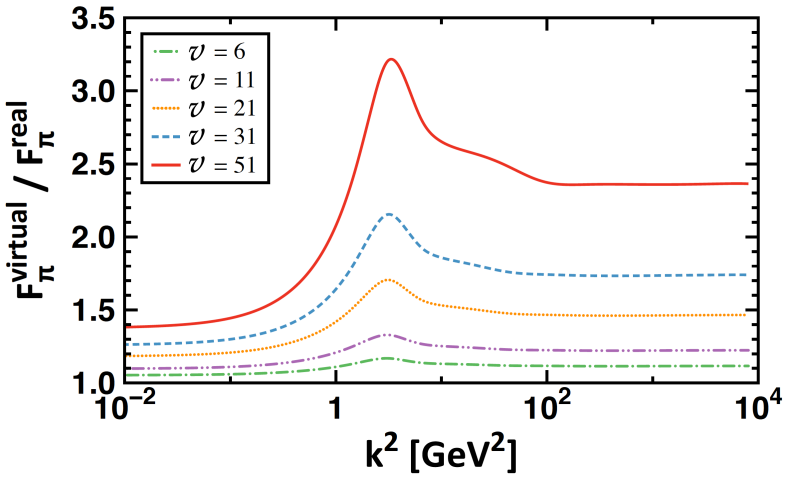

Figure 3: The virtuality-dependence exhibited by one of the UV-dominant terms in the pion's Bethe-Salpeter amplitude in [9]

1.3 Hadronic Splitting Functions in the Chiral Effective Theory

For the theoretical background, we briefly explain how to calculate the distributions in the splitting function in the KY channel. The most recent calculation is done based on Chiral Effective Theory for strange quark asymmetry [8]. Figure 4 shows all contributions to the $\bar{s}$ PDF in the nucleon from (a) the kaon rainbow and contributions to the s PDF from (b) the hyperon rainbow, and (c) kaon bubble diagrams, (d) kaon tadpole, and (e), (f) Kroll-Ruderman diagrams. The kaons, K, and hyperon, Y , are represented by the internal dashed and solid curves, respectively, and the crosses represent insertions of the operators.

The kaon rainbow distribution is shown in Fig. 4 (a). It is the light-cone distribution associated with the operator insertions on the kaon loop. Its splitting function is:

$$f_{KY}^{(rbw)}(y) = M\frac{C_{KY}^2}{f_\phi^2}\int \frac{d^4k}{(2\pi)^4}\bar{u}(p)(\not{k}\gamma_5)\frac{i(\not{p}-\not{k}+M_Y)}{D_Y}(\gamma_5\not{k})u(p)\frac{-1}{D_K^2}(2k^+\delta(k^+-yp^+)) \ , \quad (1)$$

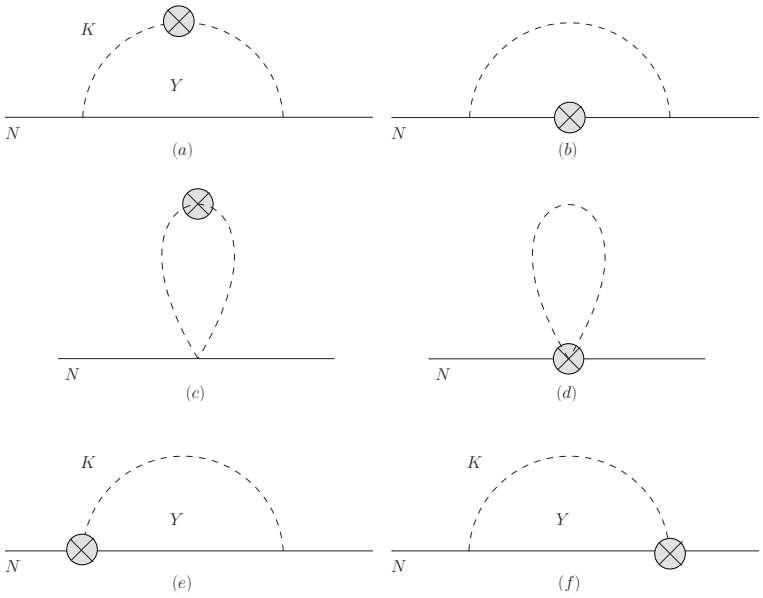

Figure 4: Contributions to the $\bar{s}$ PDF in the nucleon

where p, k are the physical nucleon and virtual kaon four momenta. D_K, D_Y are the kaon and hyperon virtualities, which are given by $D_K = k^2 - m_K^2 - i\epsilon$, $D_Y = (p-k)^2 - M_Y^2 + i\epsilon$, respectively. m_K, M_Y are the kaon and hyperon masses. $u(p)$ is spinor which is normalized by $u(p)\bar{u}(p) = 1$. C_{KY} is coefficient from effective Lagrangian, which is $\frac{D+3F}{2\sqrt{3}}$ for $K^+\Lambda$.

Decomposing terms by Dirac equation and residual theorem, the kaon rainbow distribution in "Sullivan process" can be re-written with on-shell term and contact contribution.

$$f_{KY}^{(rbw)}(y) = \frac{C_{KY}^2 \bar{M}^2}{(4\pi f_\phi)^2} \left[f_Y^{(on)}(y) + f_K^{(\delta)}(y) \right] \tag{2}$$

The on-shell term is calculated by:

$$f_Y^{(on)}(y) = y \int dk_\perp^2 \frac{k_\perp^2 + (M_y + \Delta)^2}{(1-y)^2 D_{KY}^2} F^{(on)} \ , \tag{3}$$

where D_{KY} is the kaon virtuality for an on-shell hyperon intermediate state and is calculated from $\left[k_\perp^2 + yM_Y^2 + (1-y)m_K^2 - y(1-y)M^2\right]/(y-1)$. The δ-term comes from kaons with zero light-cone momentum and is provided by:

$$f_K^{(\delta)}(y) = \frac{1}{\bar{M}^2} \int dk_\perp^2 log(k_\perp^2 + m_K^2) \delta(y) F^{(\delta)} \ , \tag{4}$$

where $F^{(\delta)}$ is the regulating function.

The coupling of the current to hyperon in the rainbow distribution which is shown in Fig. 4 (b) is calculated as in the calculation of Δ in the rainbow distribution of the π-TDIS [14] but replacing

the Δ nucleon with hyperon mass and coupling constant.

$$f_{YK}^{(rbw)}(y) = \frac{C_{KY}^2 M}{(f_\phi)^2} \int \frac{d^4k}{(2\pi)^4} \bar{u}(p)(\not{k}\gamma_5)\frac{i(\not{p}-\not{k}+M_Y)}{D_Y}\gamma^+\frac{i(\not{p}-\not{k}+M_Y)}{D_Y}(\gamma_5\not{k})u(p)\frac{i\delta(k^+-yp^+)}{D_K} . \tag{5}$$

Therefore, the total hyperon rainbow distribution function as a sum of three splitting functions associated with the on-shell, off-shell and δ-function contributions:

$$f_{YK}^{(rbw)}(y) = f_{KY}^{(rbw)}(y) + \frac{C_{KY}^2 \bar{M}^2}{(4\pi f_\phi)^2}\left[f_Y^{(off)}(y) - 2f_K^{(\delta)}(y)\right] , \tag{6}$$

where $f_Y^{(off)}(y) = \frac{2}{M}\int dk_\perp^2 \frac{M_y+\Delta}{(1-y)D_{KY}}F^{(off)}$, and $F^{(off)}$ is the off-shell regulating function.

In addition, terms involving an operator insertion at the KK_{pp} vertex and K^+ meson loop, which are called the tadpole (tad) and bubble (bub) diagrams respectively, are in fact equal and opposite [15].

$$f_K^{(tad)}(y) + f_K^{(bub)}(y) = 0 \tag{7}$$

Another key fact is that the meson-baryon rainbow diagrams (rbw) are not gauge invariant, in order to ensure gauge invariance of all the chiral loop corrections to the twist-two matrix elements requires the Kroll-Ruderman (KR) diagrams. In addition, one finds that the rainbow and KR splitting functions satisfy the identity.

$$f_{YK}^{(rbw)} + f_{YK}^{(KR)} = f_{KY}^{(rbw)} \tag{8}$$

In the end, a practical full calculation of all diagrams turns out as simple as $2\times f_{KY}^{(rbw)}$. This is exactly the same formula in the π-TDIS splitting function but with kaon virtuality, hyperon mass, its coefficient of effective Lagrangian and coupling constant.

2 Proposed Experiment

2.1 Overview

The proposed measurement together with the previously approved π-TDIS proposal (PR12-15-006), will allow the first glimpse into an essential feature of the nucleon internal structure in terms of the quark-antiquark correlation related to the meson cloud. The π-TDIS fixed-target experiment for the pion structure function at kinematics with modest momentum transfers Q^2 and higher x_{Bj} will compliment the existing HERA tagged DIS measurements. However, the proposed kaon structure function measurement will be the first time ever measurement. The proposed study of TDIS through detection of a very low energy Λ decaying into proton and π^-, which are "tagged" in coincidence with a scattered electron DIS event, will measure a very different part of the reaction space related to the long-searched-for Sullivan process for accessing the kaon structure function.

In this section we present a set of considerations concerning the Figure-of-Merit (FOM) for this experiment, a product of electron-nucleon luminosity ($\mathcal{L}$), electron detector acceptance (Ω_e), and

recoil hyperon detection efficiency (η_Λ), required for kaon-TDIS investigation. We assume a luminosity as in the approved experimental setup of π-TDIS which is constrained by the signal relative to the experimental background rates. Further details on the FOM can be found in the approved π-TDIS proposal.

In this section, we briefly emphasize the relevant aspects for the kaon measurement. The inclusive DIS cross-section for an 11 GeV electron scattering off the proton is very well known [16]. A traditional measurement of the DIS cross section with 1% precision and minimal DIS requirements on Q^2 and W^2 does not require much time with any electron spectrometer and experiments have been approved for Jefferson Lab in the 12 GeV era that will extend the existing body of such data in this kinematic regime. The (unmeasured) percentage of such events coming from the meson cloud of the proton target should be approximately 20%. The fraction of DIS events in coincidence with a low energy proton to isolate small t is smaller again than the total meson part of the nucleon wave function. Based on recent calculations [12], the fraction of DIS events with proton momenta below 400 MeV/c and at an angle within the detector acceptance (30-70^o), $F_{\pi p}(x_{Bj}, \Delta k, \Delta\theta)$ is about 1%, which is shown in Fig. 5 for the pion. From a simulation with recent calculations for the kaon, we estimated events to be a factor of 3 or 4 smaller than those for the pion. Such a small fraction leads to a low rate of true coincidence events between the DIS scattered electron and the recoiling target nucleons.

Therefore, our proposed experiment also requires good control of accidental coincidences. As it is also pointed by the π-TDIS proposal, the high rate of accidental coincidence events is the main problem for measurement of cross section. These events are mainly due to a large rate of low energy protons produced in low momentum transfer reactions, such as small angle electron elastic scattering and meson photo-production. However, the kaon-TDIS measurement requires Λ hyperon reconstruction from its decay particles, protons and pions. Therefore, applying the software cut for Λ invariant mass may clean up events from the accidental background. These following are parameters that we can optimize to reduce the accidental events:

- The Λ(p,π^-) decay angle in center-of-mass frame must be back-to-back.
- The polar angle between proton (in Λ) track and the beam direction.
- The correlation in time between an electron hit in the SBS and a proton hit in the RTPC.
- The correlation between the vertices of the electron and proton (in Λ) tracks.
- The correlation between the decay vertex of the spectator Λ (tagging the proton and pion as a target, as in BoNuS).

2.2 Kinematics

The kinematic reach of the experiment was studied using an event generator built for the Geant4 Monte Carlo simulation. The event generator used a flat distribution in $E_{e'}$ from 0-11 GeV, and a flat distribution in $\theta_{e'}$ from 5^o to 45^o and $\phi_{e'}$ of $\pm$12^o, governed by the SBS acceptance. The

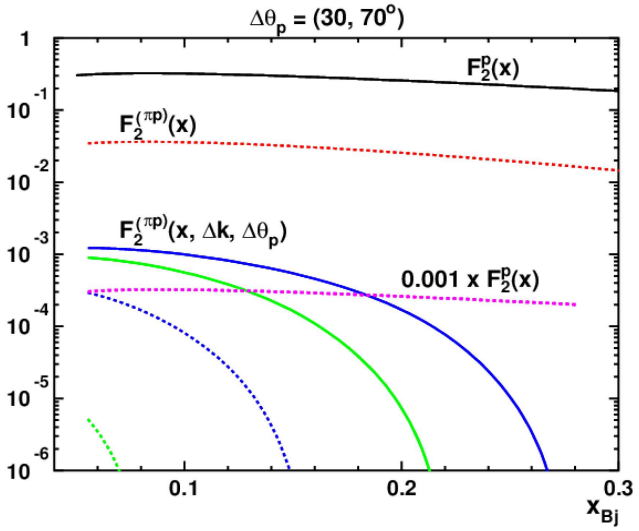

Figure 5: The proton SF, F_s^p (black), pion related $F_2^{(\pi p)}$ (red dashed), the fraction $F_2^{(\pi p)}(\Delta k, \Delta\theta_h)$ vs x_{Bj} for the proton momentum intervals, Δk (MeV/c)- green dashed (60-100), blue dashed (100-200), green (200-300), blue (300-400) and the cut on the angle between the proton and the virtual photon momentum directions, θ_p, between 30^o and 70^o. The dashed magenta line shows the level of signal for which signal to accidental ratio is 1/10, demonstrating the range of proton momentum that can be reasonably separated from the backgrounds. It also shows the x_{Bj} range over which the mesonic contribution to DIS could be measured.

x_{Bj} and the Q^2 is then calculated for the generated electrons. For the initial nucleon, the generator started with a proton at rest in the case of the hydrogen target. The transverse momentum, P_T and $z_N = \frac{q\cdot N'}{q\cdot N}$ of the recoil nucleon (where $N = p$ for pion SF, $N = \Lambda$ for kaon SF) was generated with a distribution between 50 - 500 MeV/c and 0 - 1, respectively and a flat ϕ distribution across 2π. Finally the momentum and scattering angle of the recoil proton (s), the t, y and x_π(or x_K) $= x_{Bj}/(1 - z_N)$ were calculated for the generated events. The DIS cross section is calculated as a function of x_{Bj} and Q^2 using the proton/neutron parton distributions functions in CERNLIB. The kaon-TDIS cross section was calculated similarly to the π-TDIS case using the phenomenological kaon structure function and using the relation $\sigma_{TDIS} = \sigma_{DIS} \times (f_2^{KY}/f_2^p)$. Figure 6 shows the projected kinematics of the proposed experiment for hydrogen target, where all plots have been weighted by the TDIS cross section. As noted earlier, the x_{Bj} range is determined by the low t range of interest, through the variables z_N and the low spectator momentum. This x_{Bj} range is, moreover, optimized for observation of kaons in the meson cloud. Once the x_{Bj} range is fixed, the Q^2 range obtainable with the 11 GeV beam is also determined. While the latter is not very high, the kinematics are nonetheless clearly in the deep inelastic scattering regime with W^2 values typically between 9 and 16 GeV^2. The criteria we use to optimize the x_{Bj} range for kaons is the same for the pion because of the similar sensitivity of z-dependence of the light-cone momentum distribution [17].

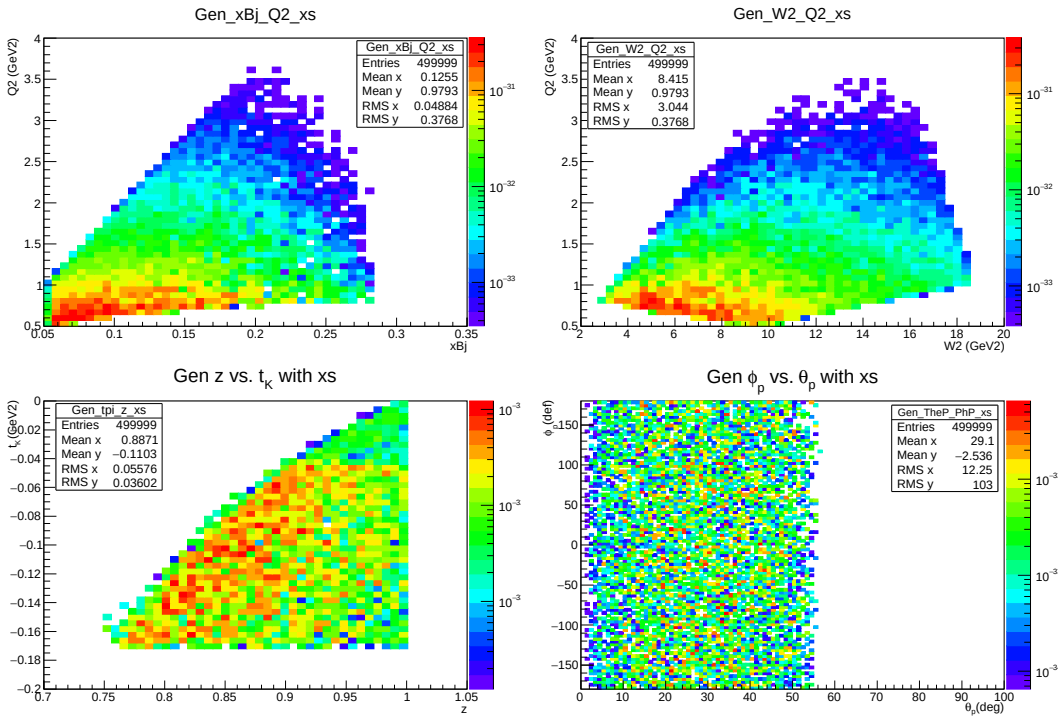

Figure 6: Kinematic coverage weighted by the kaon-TDIS cross section for $p(e, e'\Lambda)X$.

2.3 Accidental Background Rates

For the hydrogen target, there is a very high total rate of low momentum protons from low momentum transfer elastic electron-proton scattering. In the momentum range k > 70 MeV/c and luminosity 2.9$\times 10^{36}$ cm^{-2}s^{-1}, the rate is about 170 MHz. However, these protons scatter predominantly in the angular range 78-88^o. In comparison, the proton data of interest will be in a range only up to 65^o maximum. The projected polar angle resolution of the RTPC of 1^o will allow rejection of the range of angles where most of the elastically scattered protons are located. The background rate in the angular range to be used in the experiment, $30 < \theta_p < 70^o$, is relatively small (0.2 MHz) The photo-production mechanism leads to a higher rate in the angular range of interest, which was found to be about 10 MHz from the hydrogen target at the proposed luminosity of 2.9$\times 10^{36}$ cm^{-2}s^{-1} in the momentum and angular range of interest. A detailed discussion may be found in the section 2.5 "Simulation of the RTPC" of the π-TDIS proposal, PR12-15-006.

The projected time resolution of the RTPC of 10 ns allows for a narrow 20 ns timing cut in offline data analysis. The length of the RTPC target cell (40 cm), combined with the good vertex resolution of the SBS spectrometer, will provide additional suppression of accidental events by a factor of 10. However, we propose to identify the Λ from the reconstruction of the proton and pion, such an event selection will drop off accidental background significantly. Note that the determination of Λ efficiency is driven by protons. A more detailed discussion can be found in the Monte Carlo simulation section. The probability of protons to be accidentally detected in coincidence with the DIS electrons can be calculated as $P_{acc} = f_{prot} \times \tau \times (2.5\sigma_z/L)$, where f_{prot} is the singles proton

rate (around 10 MHz), τ is the timing cut/window (20 ns), σ_z is the vertex resolution (0.8 cm) and L is the length of the target (40 cm). The resulting total accidental probability is expected, then, to be 0.01 per electron. As shown in Fig. 5, the fraction of DIS events with protons within the detector acceptance with momentum < 400 MeV/c is around 1%, this implies a signal to accidental ratio of 1. However, we want to detect the lowest momentum protons that can be reasonably separated from the background. It is expected that we can extract the signal from the background for signal to accidental ratio of 1/10, this implies that we can then measure proton rates as low as 0.1% of the DIS rate (shown by the magenta line in Fig. 5).

2.4 Experimental Setup

We will utilize the same experimental setup as π-TDIS. However, in order to improve the acceptance for the proton and pion it may require optimization of the position of the RTPC with respect to the solenoidal magnetic field. A detailed explanation is provided in the Monte Carlo simulation section below. The substantial overlap between this collaboration and the π-TDIS collaboration will ensure that the apparatus is constructed and optimized to achieve the approved pion measurement, while also facilitating where possible geometry to enhance kaon events. Table 1 shows the list of input parameters and values of beam configuration and SBS and BigBite (BB) setup in the Monte Carlo simulation for this proposed measurement. The BigBite setup will help to widen range of electron kinematic coverage as planned in the pion measurement.

Table 1: GEANT input parameters for MC simulation

Beam Current	50.0 muA	BB angle	30.0^o
Target	H2	BB dist	1.55 m
Target Pressure	7.0 atmosphere	BB field	1 T
Target length	40.0 cm	HCAL angle	14.0^o
rasterx	2.0 mm	HCAL dist	6.5 m
rastery	2.0 mm	48d48 field	1
kine	tdis	48D48 dist	2.5 m
Run Time	480.0 hour	SBS Mag field	1.4 T
Beam E	11.0 GeV	RICH dist	5.0 m

2.5 Super BigBite Spectrometer: SBS

The detection of electron will be performed by the Super BigBite Spectrometer (SBS). A detailed description of the SBS setup and detector elements can be found in the π-TDIS (PR12-15-006) proposal. For this new measurement, we will keep same configuration as π-TDIS.

2.6 Recoil Detector: RTPC

Our goal for the detection requirements of the RTPC is the capability of reconstructing the Λ from its decay products, proton and pion. Based on PDG, the branching ratio of Λ decaying into proton and pion is 64%. Our detected Λ reconstruction efficiency is proportional to detection efficiency of proton by requiring the negative charged particle track in the opposite direction of ϕ in decay plane with opening angle (or opposite direction in center-of-mass frame). Detection of a soft nucleon is complicated by a large intensity of the secondary electrons, photons, and soft nucleons produced in the interaction of the high energy electron beam with the target. A RTPC proton detection option as employed by the BoNuS and CLAS eg6 experiments has several essential advantages:

- GEANT simulation shows the efficiency is driven by protons from Λ decay. (see the simulation section 3.2) Therefore, optimization of proton detection is the first priority with maximizing the detection capability of pions.
- The ionization density in the soft proton track for the momentum range 60-400 MeV/c is very high, which allows effective suppression of the secondary electron and soft photon induced signals.
- From the simulation, pion detection efficiency is a factor of 25% - 30% better than proton.
- Overall detection efficiency for both pion and proton can be improved by factor up to 2-3 by optimizing the solenoid field and z-position offset of the RTPC.
- The protons of interest (2.0 - over 30 MeV kinetic energy) have a momentum component perpendicular to the beam direction much larger than the typical perpendicular momentum of the secondary Moller electrons, which allows use of magnetic separation of the proton and electron background using a solenoidal magnet.
- The proton in combination with negative pion track allows for reconstruction of the event vertex and direction, which are a powerful means for rejection of accidental events.
- The proton detector readout segmentation could be on the level of 10^5 or above.

The recoil detector will be the similar as the cylindrical RTPC being developed for the experiment to measure the structure function of the free neutron (E12- 06-103, or BoNuS-12), the latter being based on the very successful cylindrical RTPCs that were employed for the BoNuS and CLAS eg6 experiments as pictured in Fig. 7. The proposed RTPC will, however, utilize a different solenoid with a 400-mm warm bore, a total length of 152.7 cm, and a superconducting coil that operates with a 4.7 T magnetic field in the center of the magnet (see Fig. 8). This solenoid belongs to the UVa collaborators on this proposal, and is currently being used for tests of LHC detector electronics. Any stray field of the solenoid on the asymmetric iron of the SBS, could be symmetrically balanced with an iron yoke. While this approach certainly needs a full analysis for exact design, we note that this is reasonably standard, and that a solenoidal field surrounded by an iron yoke is typical for collider geometry. The heating of the superconducting coil is not expected to be an issue for this proposal because of the relatively small luminosity and the coil being immersed in liquid He.

Simulation studies have shown that increasing the radial drift region by a factor of 2 compared to the BoNuS and eg6 RTPC detectors can provide at least a 50% relative improvement in the momentum resolution, as well as extending the momentum range of the detector. The larger bore of this magnet will facilitate the RTPC having a larger radial drift distance than that proposed for BoNuS-12. The enhanced drift region will facilitate measurements of proton momenta up to 400 MeV/c with a resolution of 3%. The length of this magnet is also a help, allowing us to use a longer (40 cm) target for improved background rejection and luminosity. The proposed TDIS RTPC will be 40 cm long and consist of an annulus with inner radius of 5 cm and an outer radius of 15 cm. The amplification of the drifting electrons will be achieved by three layers of cylindrical Gas Electron Multiplier [18].

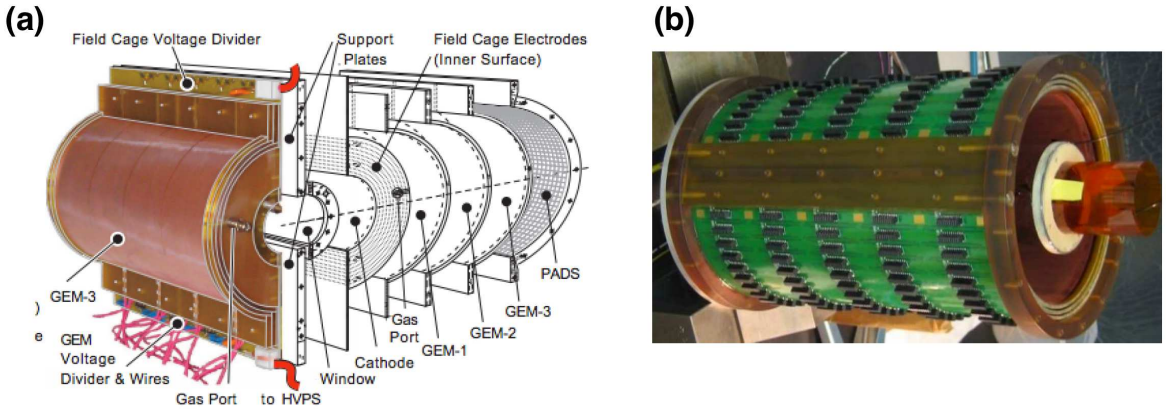

Figure 7: (a) Schematic drawing of the BoNuS RTPC, showing the left module with the readout pad-board removed and a complementary exploded view exposing the components of the right module. (b) Photograph of the eg6 RTPC during assembly

To read out signals from the detector, we expect to use the DREAM chip based Scalable Readout System (SRS) recently developed by the Saclay group. This offers the time range we need and gives the flexibility to optimize parameters as needed for this experiment. A time resolution as low as 4 ns was recently demonstrated [19] in the LHCb GEM chamber with a similar readout where the GEM signal was firstly integrated and then digitized. This technology is rapidly developing and the π-TDIS collaboration may choose an option with even better performance than the DREAM chip. Any option that π-TDIS will find acceptable will work for this proposal as well.

3 Monte Carlo Simulation

3.1 Event Generator

We developed a stand-alone event generator to produce the event of $H(e, e'\Lambda)X$ reaction based on the chiral effective theory for strangeness quark asymmetry. In the calculation, all Feynman

diagrams that we discussed in Sec. 1.2 are included with two possible regularization forms in the splitting function. We took into account a model dependent coupling constant, $g_{K^+p\Lambda}$ which is calculated in the GPDs framework [20]. Each physics event is generated in phase-space and weighted by kaon-TDIS cross-sections. Actually the Λ coupling parameter is kind of an upper limit cut-off because of the unknown s quark PDF. Therefore what we measure in experiment is in fact to provide a better constraint. The event generator is then plugged into g4SBS simulation package. We estimated event rate for kaon-TDIS using a given experimental configuration from π-TDIS proposal.

3.2 Simulation of RTPC

The RTPC detector simulation of the detection probability of $H(e, e'\Lambda)X$ reaction has been carried out using a simulation based on a recent release of Geant-4 (4.10.01.p02) [21]. Figures 8 and 9 show the magnetic field strength as a function of R, z and a snapshot of the RTPC geometry in GEANT4 simulation. The magnetic field is input to the Geant-4 simulation using a TOSCA field map of the UVa solenoid. We consider in the simulation a "straw" type target of radius 5 mm and length 400 mm, held in a 10 μm thick Al cylinder, with 20 μm Be end-cap windows, and filled with 7 atm of H2 or D2 gas. This cell is surrounded by the He gas of the RTPC, at a pressure of 0.15 atm, contained within a volume of 150 mm radius. Both the straw target and the He volume are maintained at a temperature of 77^{o}K. A ring of 127 μm radius, gold-plated Al field wires divides the He volume into an insensitive region (He-inner) at radii $r < 50$ mm and a sensitive region (He-outer) at radii $50 < r < 150$ mm. The electrons of ionization produced in He-inner region are swept to the target cell and the ions collected by the wire ring. Ionization produced in He-outer is moved by the radial electric field to an outer ($r >$150 mm) triple GEM detector with pixel readout. The density of the He gas in the RTPC has been fixed at 9.75×10^{-5} g/cm^3 which corresponds to a pressure of 0.15 atm at 77^{o}K. A detailed simulation with regarding to general operation of RTPC and target configuration are the same and explained in [12]. Figure 10 shows an example of Λ event in BoNuS type RTPC using our event generator. It has a 100 MeV/c momentum of Λ decays to proton and π^-. Both proton and pion clearly leave their tracks in the gas volume and a well observable opposite track pattern. Even a forward going Λ event (this example in the figure) can be reconstructed due to its decay with opening angle between pion and proton. Note that the BoNus type RTPC has a shorter drift radius (40mm) due to the detector space limit.

Particle Identification in the analysis of step-by-step information along particle tracks produced by the simulation have been analyzed to determine dE/dx in the RTPC gas for p, π^+, K^+, e. Particles have been produced at angles θ= 30-70^o, at position $z = 0.0 \pm 5$ mm, and at momenta p_{inc} of 100$\pm$1, 250$\pm$1 and 400$\pm$1 (MeV/c). Figure 11 shows the resulting distributions at 250 MeV/c, for tracks with a total length greater than 50 mm. The dotted line in the figure shows the position of the cut used to select proton events. Overall acceptance and dE/dx characteristics has been addressed in Table 5 of the pion proposal [12]. From the plot shown here, proton acceptance is 95.5%, kaon contamination is 1%, π^+ contamination is 0.04% and e contamination is 0%. Note that this Mean and RMS estimation of dE/dx in Fig. 11 were based on 100mm of radius of RTPC gas drift however it is plotted in 1mm increments only, which we can improve the resolution. Thanks to the large radius of RTPC design, the maximized effective track length will be factor of 4

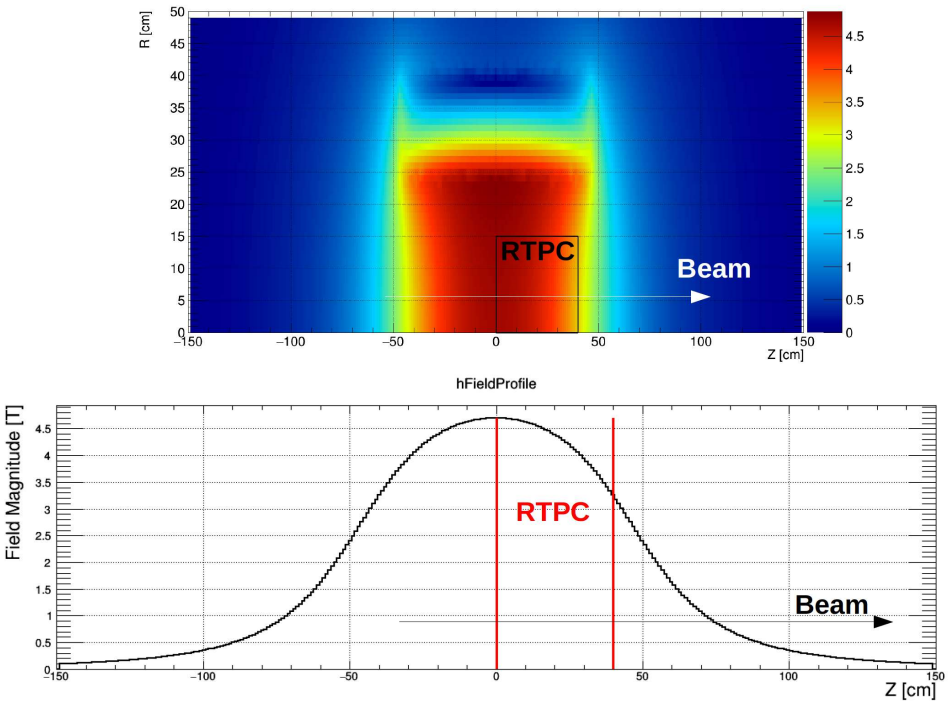

Figure 8: Nominal field conditions are as shown below, with the RTPC offset by +200mm from the solenoid centre to reduce background in beam exit region

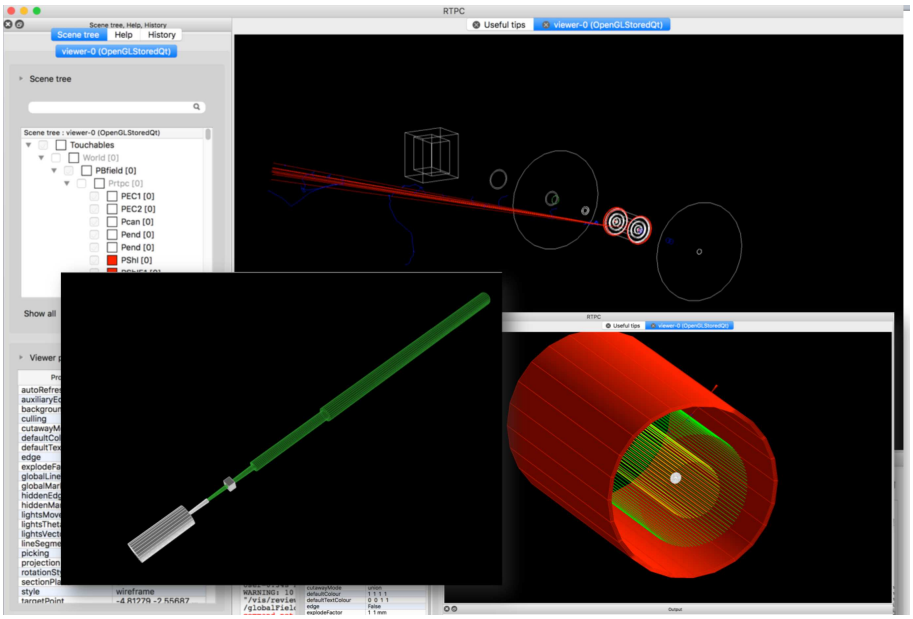

Figure 9: RTPC design and setup in the GEANT4 simulation package with 10 events of 150 MeV/c protons at θ=90^o.

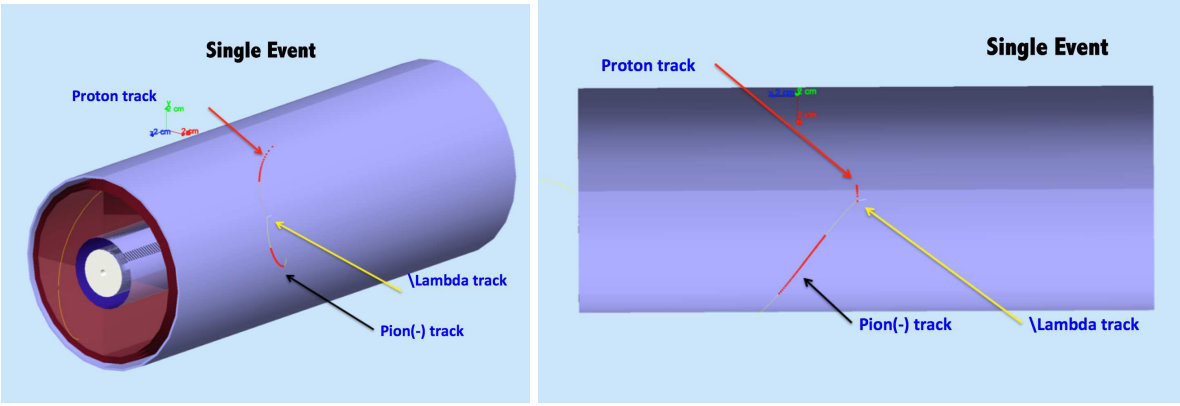

Figure 10: An example of Λ particle track in GEMC and its decay products: proton and π^- in RTPC (BoNuS12 design). The red dots are hits along the proton and pion tracks in the active region of the RTPC.

larger. Such a long track is a beneficial and this allows us to change an increment with 2mm, 4mm or 5mm. Such increasing distance unit will improve its resolution significantly. We will evaluate this through the simulation and optimize.

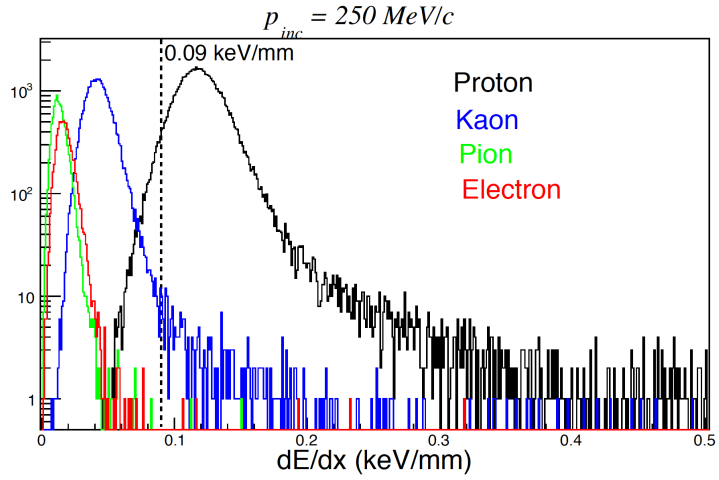

Figure 11: The energy deposition in path length, dE/dx for particles of momentum 250 MeV/c detected in the outer He volume of the RTPC.

In order to make projections, we generated the events of $H(e, e'\Lambda)X$ from our event generator and utilized the g4SBS simulation packages. We generated 500k events in total with given experimental configuration which is given in Table 1. We counted the number of events that produce tracks in the RTPC and recorded by the RTPC GEANT4 simulation, so call "track probability". We also generated the $H(e, e'p)X$ with same beam time and experimental configuration for comparison. We summarize this probability with various RTPC geometrical offsets in table 2. Overall, for $H(e, e'\Lambda)X$ reaction with Λ decay to proton and pion, the probability of detecting a track for pro-

tons, pions in RTPC gas volume are 40%, 52%, respectively. The probability that both proton and pion make tracks in the event is 33-37%. We also estimated the track probability for $H(e,e'p)X$ event as you see in last columns of table 2. As expected, the tracking probability for $H(e,e'\Lambda)X$ is almost 50% lower than one for $H(e,e'p)X$, because of the difference between three-body and two-body systems as well as more high momenta of protons in $H(e,e'p)X$ reaction. However, it is clear that an optimization of the RTPC offset with respect to the solenoid field improves the tracking probability for both $H(e,e'p)X$ and $H(e,e'\Lambda)X$ reactions. Note that this improvement is achieved by only optimizing z-offset of RTPC. There are many parameters (e.g. gain, gas pressure, gas mixture, RTPC readout,...) we can adjust to further improve the efficiency.

Table 2: Probability of creating a track of particle in RTCP gas volume (%)

Reaction / Offset(mm)	$H(e,e'\Lambda)X$	$H(e,e'p)X$
tracked particle type	(p:π^-:$p\pi^-$)	(p)
0	(40:50:33)	74.4%
100	(40:50:33)	74.6%
200 (nominal)	(40:52:35)	74.6%
500	(40:54:36)	75.7%
600	(40:54:37)	75.9%
1000	(41:55:38)	75.8%

We apply detector effects of RTPC - all 3-momenta were smeared by Gaussian smearing with a resolution of 3% which we used from the π-TDIS proposal. We did not apply any smearing to energy in 4-momenta. We did not apply the acceptance and efficiency cuts either, which is stated "conservative and combined RTPC acceptance and efficiency of 40% " in the π-TDIS, because this geometrical acceptance and particle detection efficiency should be reaction independent. Figure 12 shows the invariant mass of events with both protons and pions detected in RTPC (black curve) and taking into account 3% of momentum smearing (red curve).

Beyond the simulations described above, and since the π-TDIS studies, further simulations of the RTPC detector itself and the optimization of its efficiency are underway. Geant-4 itself is not ideal for simulating the drift and diffusion of the low-energy ionised electrons created within the RTPC drift volume, and so this has separately been studied using the software package, called Garfield^{++} [22]. It is a toolkit for simulating detectors incorporating gas or semi-conductors as the sensitive medium, and is commonly used to simulate electron drift in gases under the influence of magnetic and electric fields. Using this toolkit, electron drift paths and times within the RTPC volume have been studied, for different gas mixtures and electric field set-ups. Drift times on the order of 20 μs are achievable with the proposed nominal drift-region gas mix of He:CH_4 in a 90:10 ratio, maintained at 0.15 atm and 77 K. However through further studies of gas mixes, temperatures, pressures and electric field magnitudes this could be optimized if required. An instance of the Garfield^{++} simulation has additionally been embedded within the Geant-4 TDIS simulation. Within this framework the tracked particle, for example proton, is killed when it enters the RTPC He volume. Physics process are then controlled by Garfield^{++}, which handles the set-up of the gas properties, electromagnetic field and simulates the drift electrons' trajectories. These simulations

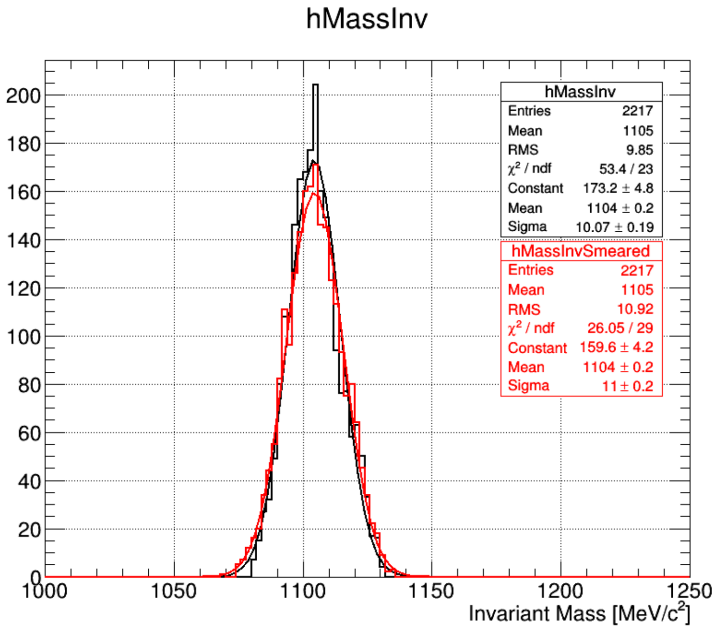

Figure 12: Λ mass reconstruction from decay particles: protons and pions with taking into account 3% of Gaussian smearing in RTPC resolution.

will continue, as they are useful for tracking studies, to determine expected readout occupancies and fine tune the drift region properties if required.

Advancements to the TDIS geometry within the Geant-4 framework have also been made and will continue. For example, a curved exit window for the target and a curved spherical Al exit-wall to re-enforce the mechanical integrity of the RTPC have been implemented, to allow for studies of different pressure set-ups. Additionally, more beam-line material and extra casing surrounding the external volume of the recoil detector have been added. The capability to scale the magnetic field map input has been implemented, which will also be useful for both π-TDIS and kaon-TDIS efficiency studies as a function of the solenoid current. For a better comparison with the π-TDIS simulation results these additions have not been included in the results shown here, but geometry matching the π-TDIS simulations was used. Therefore, in principle we can carry out the experiment with the configuration of π-TDIS, but what we are performing for optimizations (because the better Λ reconstruction efficiency the better protons reconstruction efficiency) that will benefit both measurements.

4 Projected Results

4.1 Beam Time Request

We propose to measure the semi-inclusive reaction of $p(e, e'\Lambda)X$ using the same experimental condition in the π-TDIS proposal, 50μA beam on a 7 atm, cooled straw, gaseous hydrogen target with radius of 5 mm and length of 40 cm, for a total luminosity of 3×10^{36} cm^{-2}s^{-1}. The well-known DIS cross section was used as the initial basis for calculation [23], in conjunction with the rate due to the kaonic contribution is given by: Rate(DIS$_{KY}$) = Rate(DIS)$\times(F_{KY}^2/F_n^2)$. The tagged-DIS rate on hydrogen is given by: Rate(TDIS$_{KY}$) = Rate(DIS)$\times$ eff$_{RTPC}$ $\times$eff$_{SBS}$. Using a conservative combined RTPC efficiency (eff$_{RTPC}$) and acceptance of 40% and SBS efficiency (eff$_{SBS}$) of 90%. The x_{Bj} range $0.06 - 0.2$ will be divided into 5 bins and, for each bin in x_{Bj}, the recoil Λ momentum k will be divided into at least another 6 bins. This is same binning and kinematic coverage of [12].

The requested beam time for this measurement is basically same as the π-TDIS but make sure the given beam time satisfies the goal of better than 2-3% statistical uncertainty on average for the recoil momentum k bins within each x_{Bj} bin. The estimated electron cross section within the SBS acceptance, the F_{KY}^2/F_n^2, the projected TDIS rate, and the yield in each x_{Bj} bin for 10 days of beam on a hydrogen target is roughly factor three smaller than one in the Table 6 on π-TDIS proposal. This reduction factor reflects in the projected result in Fig. 14. Statistics are estimated in each kinematic E', θ, ϕ bin with cuts on the SBS acceptance, and an electron trigger energy < 6 GeV, and threshold > 1 GeV. In addition, kinematic cuts for DIS employed to ensure $W > 2$ and $Q^2 > 1$ GeV^2.

The electron yields, $N_{e,e'}$, are based on well known DIS cross section [23], the yields for the protons of interest is estimated as $N_{e,e'\Lambda}^{good} = N_{e,e'} \times (F_{KY}^2/F_n^2)$, the accidental proton yields $N_{e,e'\Lambda}^{acc}$, are based on the same background simulation from $N_{e,e'p}^{acc}$. Finally the statistical uncertainty is estimated as $\delta\sigma = \sqrt{N_{e,e'\Lambda}^{good} \times (1 + B/S)}$, where S/B is the signal to background ratio. In addition to 10 days of 11 GeV beam on hydrogen and 10 days on deuterium, we request also 5 days on a hydrogen target at a reduced luminosity in order to validate the background subtraction procedure. It will be necessary to commission the RTPC, the new SBS electron detection system, as well as to verify the vertex and reconstruction optics. We request 2 beam days (mixed evenly between the hydrogen and deuterium targets), also at 11 GeV, for these requisite preparations. We note that the collaboration anticipates some advance detector pre-commissioning of the RTPC and SBS detectors using radioactive sources, cosmic rays, and possibly the low energy proton beam at TUNL as was done in advance for BoNuS.

Figure 13 depicts the potential reach in t of $F_2^{(\pi p)}(t, \Delta x)$ (left) and $F_2^{(K\Lambda)}(t, \Delta x)$ (right) towards pole positions for a number of different x_{Bj} bins. Here, it is solely true for both $F_2^{(K\Lambda)}$ and $F_2^{(\pi p)}$ that the low momentum reach of the RTPC detector is critical to define the downward-turning shape of the curve. Although x-axis scale is different between left and right plots in Fig. 13, it clearly shows that the kaon structure function has less sensitivity of x_{Bj} range than the pion structure function. As we explained in the previous section 1.2, this may be explained in the context of the

relative importance of the pion and kaon pole. However, recent calculations estimate that the kaon can serve as a valid meson target up to $-t < 0.9$ GeV^2 [9].

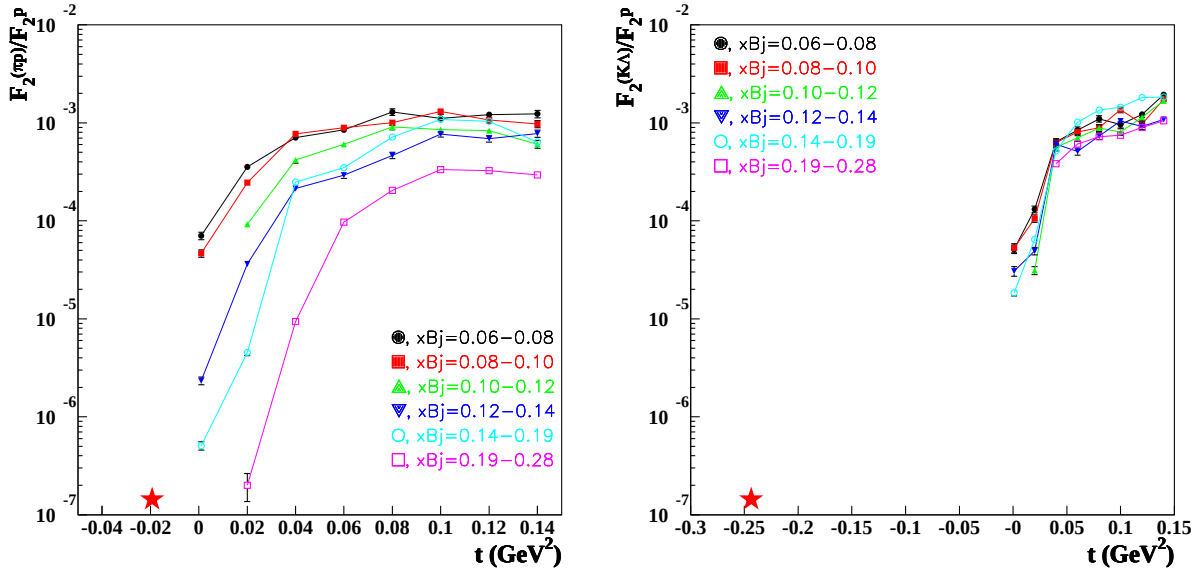

Figure 13: t dependence of the ratio of $F_2^{(\pi p)}(t, \Delta x)/F_2^p$ with momentum cut 100 - 400 MeV/c (left) and $F_2^{(K\Lambda)}(t, \Delta x)/F_2^p$ with minimum momentum cut $<$ 100 MeV/c (right), for varying ranges in x_{Bj}. The projections include the statistical error , which are of the size of the symbols. The red stars show the location of the pion and kaon poles.

The proposed experiment will provide access to the kaon structure function via the Sullivan process, where the coincidence of the DIS-scattered electron and the low momentum recoil Λ will tag a kaon target event. Experimental knowledge of the partonic structure is limited and data exist only for the pion in the valence region from pionic Drell-Yan scattering. There is a complete lack of kaon data. Fig. 14 shows the projected pion (left) and kaon (right) valence quark distribution as a function of x_π (or x_K) that extracted from this proposed measurements. A 5% systematic uncertainty in the pion flux is assumed (to be achieved by comparing to pionic Drell-Yan data at x_π = 0.5), and a total systematic uncertainty of 8.4% is used.

4.2 Expected Experimental Accuracy

We estimate an overall systematic uncertainty with 5% in the cross section measurements, which is similar to one for the π-TDIS proposal. Although we have factor of 3 lower statistics than $F_2^{(\pi p)}$ measurement. First, CLAS-6 had a large ($> 5\%$) uncertainty associated with the E', θ dependent CLAS trigger efficiency. The SBS is a far simpler device, and is expected to have a very small trigger efficiency uncertainty and only a 3% overall systematic uncertainty. In BoNuS, moreover, 4.2% of the 8.7% overall systematic uncertainty came from the inclusive $F_2^d = F_2^p$ model dependence in the ratio measurement performed largely in the resonance region. We are here proposing

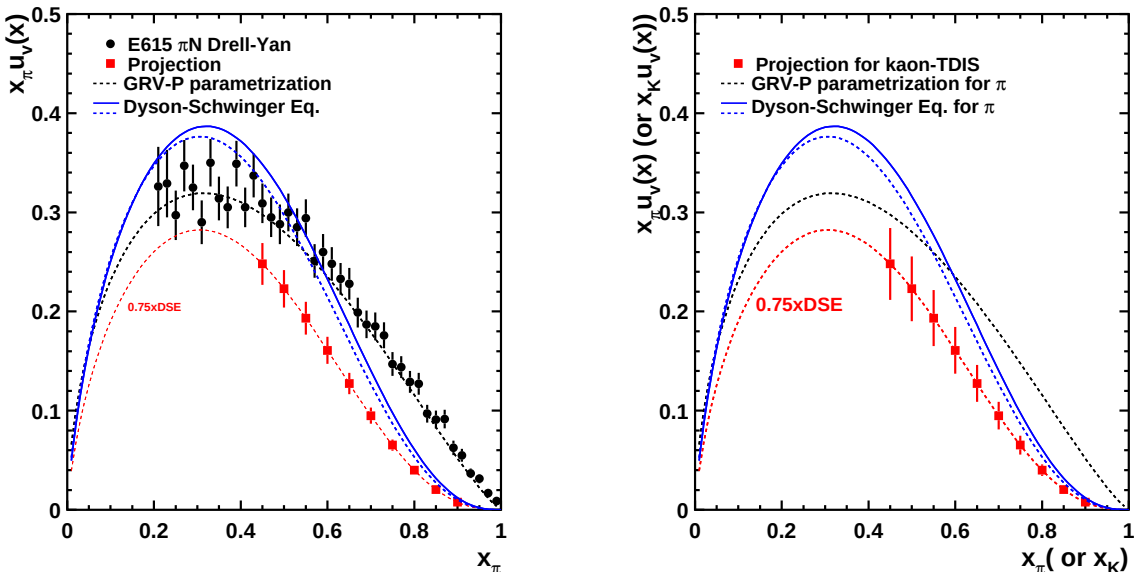

Figure 14: Projected pion (left) and kaon (right) structure function results (red solid squares). All results from the Drell-Yan experiment E615, the GRV-P parametrization and a Dyson-Schwinger equation calculation are for pions only. The projected points are shown along a curve which is 0.75×DSE, in order to demonstrate the potential for shape discrimination.

a cross section measurement, with no ratio normalization technique to be employed. SBS inclusive results can be verified against the well-known proton DIS cross section. Moreover, the better spatial resolution of the proposed GEM readout, combined with the increased drift distance, will improve tracking and vertex resolution in the RTPC as compared to BoNuS.

From a background analysis based on the real coincidence between the DIS electron and secondary mesons misidentified as protons, the uncertainty on the pion contribution to the electron sample is expected to be on the level of 1% or less. Secondary mesons misidentified as protons can be determined with a 10% uncertainty, which implies a 1% uncertainty in the true coincidence counts. The uncertainty for the PID by dE/dx and coincidence is estimated to be 1%. This is based on the energy deposition in path length and the discussion in the pion-TDIS proposal. The anticipated impact on the systematic uncertainty due to backgrounds is expected to be small due to several available methods which are proposed to evaluate them. For example, a coincidence time cut and a vertex (δz) cut will be used. Low luminosity data taking (5 PAC days requested for these studies) will also be used to verify the simulations and calculations from the higher rate data. This is included in the systematic uncertainty in table 3

Table 3: Estimation of systematic uncertainties (%)

source	uncertainty
Accidental background subtraction	5.0
PID by dE/dx and coincidence	1.0
DIS electron cross-section (Target density, Beam charge, Acceptance, Det.eff.)	3.0
RTPC absolute eff.	2.0
RTPC deadtime	1.0
RTPC momentum resol.	$<$1.0
RTPC angular accept.	1.0
Total	6.5

5 Summary

We propose to measure the semi-inclusive reactions $H(e,e'\Lambda)X$ in the deep inelastic regime of W^2= 8 - 18 GeV^2, Q^2= 1 - 3 GeV^2, and x_{Bj}= 0.05 - 0.2, for very low Λ momenta in the range 60 MeV/c up to 400 MeV/c. This is exactly the same kinematic region that was proposed by π-TDIS. The experimental apparatus will consist of the Hall A Super BigBite Spectrometer for identification of electrons with a low density target (gaseous hydrogen, deuterium), and, a radial time projection chamber (RTPC) with GEM-based readout, inside a large bore diameter 5T solenoid. These new detector packages along with the CEBAF high current CW beam, leverage the high luminosity (3×10^{36} cm^{-2}s^{-1}) necessary to access the proposed physics. The key to this experimental technique is to measure the low-energy outgoing "recoil" proton and pion from Λ decay in coincidence with a deeply inelastically scattered electron from the hydrogen target. The proposed experiment will be a first ever measurement to directly access the elusive kaon structure function. The inclusive electron kinematics determine that a DIS event has occurred, i.e. that the reconstructed Q^2 and missing mass, W^2, of the recoiling hadronic system are sufficiently large. However, unlike the standard inclusive case, the low momentum protons measured in time and vertex coincidence with the DIS event ensure that the deep inelastic scattering occurred from partons within the meson cloud (here identified as a kaon) surrounding the nucleon. This can be achieved by employing the Super BigBite Spectrometer to detect the scattered electrons in time and vertex coincidence with low momentum proton(s) measured in a low mass radial time projection chamber. The proposed kaon structure function measurement can be achieved, although with lower statistics, in parallel with the pion structure function measurement. This is a crucial measurement not only for the physics interest, but also to understand an important background to the pion TDIS proposal.

References

[1] S. Catani *et al.*, Phys. Rev. Lett. **93**, 152003 (2004).

[2] A. W. Thomas, Phys. Lett. B **126**, 97 (1983).

[3] M. Arneodo *et al.*, Phys. Rev. D **50**, 1 (1994).

[4] K. Ackerstaff *et al.*, Phys. Rev. Lett **81**, 5519 (1998).

[5] A. Baldit *et al.*, Phys. Lett. B **332**, 244 (1994).

[6] R. S. Towell *et al.*, Phys. Rev. D **64**, 052002 (2001).

[7] A. I. Signal and A. W. Thomas, Phys. Lett. B **191**, 205 (1987).

[8] X. G. Wang *et al.* arXiv:1610.03333 Oct. (2016).

[9] S. Qin, C. Chen, C. Mezrag, and C. D. Roberts, arXiv:1702.06100, (2017).

[10] J. Badier *et al.*, [NA3 Collaboration] Phys. Lett. B **93**, 354 (1980).

[11] T. Nguyen, A. Bashir, C. D. Robert and P. C. Tandy, Phys. Rev. C **83**, 062201 (2011).

[12] C. Keppel, J. Annand, D. Dutta, P. King, B. Wojtsekhowski *et al.* PR12-15-006 "Measurement of Tagged Deep Inelastic Scattering(TDIS) (2015).

[13] J. D. Sullivan, Phys. Rev. D **5**, 1732 (1972).

[14] J. R. McKenney, N. Sato, W. Melnitchouk, C. R. Ji, Phys. Rev. D **93**, 054011 (2016).

[15] C. R. Ji, W. Melnitchouk and A. W. Thomas, Phys. Rev. D **88**, 076005 (2013).

[16] C. Patrignani *et al.* (Particle Data Group), Chin. Phys. C **40**, 100001 (2016).

[17] H. Holtman, A. Szczurek and J. Speth, Nucl. Phys. **A596**, 631 (1996).

[18] F. Sauli, Nucl. Instrum. Meth. **A386**, 531 (1997).

[19] Dead-timeless readout electronics ASIC for Micromegas

[20] P. Kroll, S. Goloskov, Eur. Phys. J **A47**, 112 (2011).

[21] S. Agostinelli *et al.*, Nuclear Instruments and Methods in Physics Research **A506**, 1533 (2003),

[22] `https://garfieldpp.web.cern.ch/garfieldpp/`

[23] L. W. Whitlow, E. M. Riordan, S. Dasu, S. Rock, and A. Bodek, Phys. Lett. B **282**, 475 (1992).